Probabilistic risk assessment of earth dams with spatially variable soil properties using random adaptive finite element limit analysis

Kang Liao[1,2], Yiping Wu[1,*], Fasheng Miao[1], Yutao Pan[3], Michael Beer[2]

[1]Faculty of Engineering, China University of Geosciences, Wuhan 430074, China

[2]Institute for Risk and Reliability, Leibniz University Hannover, Hanover 30167, Germany

[3]Department of Civil and Environmental Engineering, Norwegian University of Science and Technology, Trondheim 7491, Norway

* Corresponding author: ypwu@cug.edu.cn (Yiping Wu)

E-mail address: kangliao@cug.edu.cn (Kang Liao), ypwu@cug.edu.cn (Yiping Wu), fsmiao@cug.edu.cn (Fasheng Miao), yutao.pan@ntnu.no (Yutao Pan), beer@irz.uni-hannover.de (Michael Beer)

Abstract

Risk assessment of earth dams is concerned not only with the probability of failure but also with the corresponding consequence, which can be more difficult to quantify when the spatial variability of soil properties is involved. This study presents a risk assessment for an earth dam in spatially variable soils using the random adaptive finite element limit analysis. The random field theory, adaptive finite element limit analysis, and Monte Carlo simulation are employed to implement the entire process. Among these methods, the random field theory is first introduced to describe the soil spatial variability. Then the adaptive finite element limit analysis is adopted to obtain the bound solution and consequence. Finally, the failure probability and risk assessment are counted via the Monte Carlo simulation. In contrary to the deterministic analysis that only a factor of safety is given, the stochastic analysis considering the spatial variability can provide statistical characteristics of the stability and assess the risk of the earth dam failure comprehensively, which can be further used for guiding decision-making and mitigation. Besides, the effects of the correlation structure of strength parameters on the stochastic response and risk assessment of the earth dam are investigated through parametric analysis.

Keywords: Risk assessment; Spatial variability; Random adaptive finite element limit analysis; Random field theory; Monte Carlo simulation

Article Highlights

(1) The methods of probabilistic risk assessment of earth dams in spatially variable soils are clarified in the framework of random adaptive finite element limit analysis.

(2) The statistical characteristics of the stability and quantitative risk assessment of the earth dam considering the soil spatial variability are studied.

(3) The effects of the correlation structure of strength parameters on the stochastic response and risk assessment of the earth dam are investigated.

1. Introduction

Earth dams composed of soils and rock debris are a type of commonly seen geo-structures in the word, which have attracted increasing attention because of the serious consequences of their destruction [1]. The soil properties in the earth dams generally exhibit a certain spatial variability even within homogeneous layers as a result of depositional and post-depositional processes [2]. The existence of spatial variability increases the complexity of evaluating dam stability [3, 4]. From an engineering perspective, the concern is not only the stability of an earth dam, but also the consequence of its failure. The risk assessment accounts for the probability of failure as well as the corresponding consequence simultaneously [5]. In this case, the effects of the soil spatial variability on the risk assessment of earth dams can be more profound since the consequences associated with different failure modes are individual [6]. However, a majority of analyses assume that the material properties applied to soil layer are deterministic, and a monotonous factor of safety with minimum information is obtained. These conventional deterministic methods ignore the soil spatial variability, which deviate from the actual stability and risk. Therefore, it is more rational to take the spatial variability of soil properties into account when assessing the stability and the risk of earth dams, otherwise the results can be distorted.

At present, the spatial variability of soil properties is often described by the random field theory for stochastic analysis [7]. Random finite element method (RFEM) which incorporates the random field theory and the finite element method has attracted widespread attention in the field of geotechnical engineering by dint of its promising performance [8-11]. In the context of RFEM, the spatial variability can be well characterized by a random field of the parameters of interest and then mapped onto the partitioned finite element mesh [12, 13]. Although the RFEM has the ability to deal with the problems of random variables with spatial variability and produces a seemingly reasonable solution, the results obtained greatly depend on the size of the mesh and may lead to an undemanding factor of safety and consequence owing to unsuitable meshing [14, 15].

Alternatively, the random adaptive finite element limit analysis (RAFELA) is developing rapidly in recent years, which can give precise ultimate solution by imposing the adaptive meshing within the finite element limit analysis [16]. Unlike RFEM which manually divides the mesh and gets a single solution, RAFELA relies on adaptive meshing technique and brackets the solution by strictly close lower bound (LB) and upper bound (UB). This approach greatly improves the calculation accuracy through generating the mesh automatically, which can be applicable to complicated structures that RFEM may not be well competent even with a sufficiently dense mesh because of the irregular geometry [17]. Nowadays, RAFELA has become a powerful tool to deal with a variety of stability problems where the soil properties are spatially variable [18-20], but it has rarely been reported in quantifying the dam stability and risk assessment.

In this study, RAFELA is employed to assess the risk of an earth dam failure where the spatial variability of the strength parameters is involved. This state-of-the-art technique integrates the random field theory and adaptive finite element limit analysis (AFELA) in a Monte Carlo simulation (MCS) framework. At first, the random fields of the strength parameters are discretized by the Karhunen–Loève expansion (KLE). Then the bound solution and the corresponding consequence are obtained by the AFELA. Subsequently, the probabilistic risk assessment of the dam failure is quantified via the MCS. Furthermore, a series of parametric analyses with regards to the correlation structure of the strength parameters are discussed.

2. Methodology

2.1 Adaptive finite element limit analysis

Finite element limit analysis (FELA) embedded with adaptive meshing, also termed as AFELA, is a powerful tool newly developed for evaluating the performance of the geotechnical structures. The former inherits the advantages of the finite element method and limit theorem providing a variety of modeling environments and strict bound solution. The latter can produce adaptive meshes automatically in an optimal way to maximize accuracy while keeping the computational cost at a minimum [16, 21, 22].

According to the bounding theorems of classical plasticity that assume the material to be perfectly plastic and follows an associated flow rule, LB and UB solutions can be evaluated by constructing a reasonable statically admissible stress and kinematically admissible velocity fields, respectively. Considering a structure of rigid plastic material with volume V is subjected to a set of body forces $\boldsymbol{b}$ while a set of tractions $\boldsymbol{t}$ are acting on its boundary. As shown in Fig. 1, the displacements are prescribed on left of the boundary S_u, while the tractions are prescribed on the right part of the boundary S_σ. $\boldsymbol{n}$ is the outward normal to the boundary. For such a scenario, the limit analysis can be described as the maximum magnitude of the tractions that can be sustained without the structure suffering collapse or the minimum magnitude of the tractions that will cause collapse.

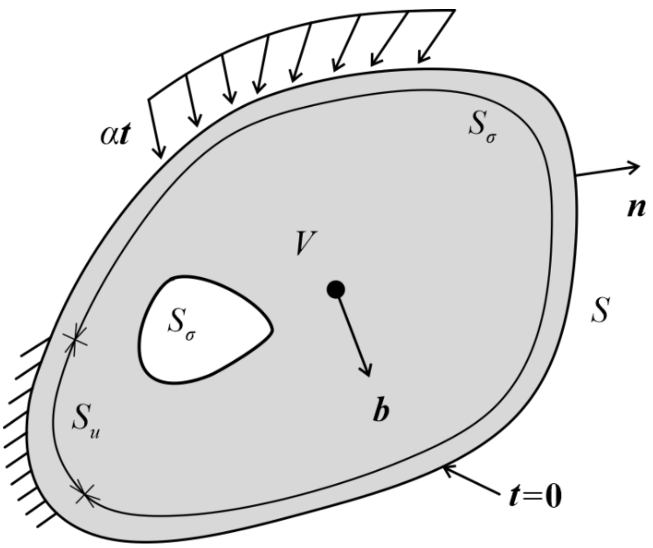

Fig. 1 Surface and body forces acting on a structure of rigid plastic material

To answer this question, a load multiplier α is introduced to describe the tractions acting on the structure which are given by $\alpha\boldsymbol{t}$. Mathematically, the solution within the limit analysis framework should satisfy the following governing equations:

1. The equilibrium and static boundary conditions:

$$\begin{aligned} &\nabla^{\mathrm{T}}\boldsymbol{\sigma}+\boldsymbol{b}=\mathbf{0} &&\text{in } V \\ &\boldsymbol{A\sigma}=\alpha\boldsymbol{t} &&\text{on } S_{\sigma} \end{aligned} \tag{1}$$

2. Yield conditions:

$$\boldsymbol{F}\left(\boldsymbol{\sigma}\right)\le 0 \tag{2}$$

3. Associated flow rule assuming infinitesimal strains:

$$\boldsymbol{\varepsilon}=\nabla\boldsymbol{u}=\boldsymbol{\lambda}\nabla\boldsymbol{F}\left(\boldsymbol{\sigma}\right) \tag{3}$$

4. Complementary conditions:

$$\boldsymbol{\lambda F}\left(\boldsymbol{\sigma}\right)=0,\ \boldsymbol{\lambda}\ge 0 \tag{4}$$

where $\boldsymbol{A}$ denotes an equilibrium matrix, $\boldsymbol{\sigma}$ denotes a vector of stresses, ∇^{T} denotes the equilibrium operator (∇ being the strain-displacement operator), $\boldsymbol{F}$ denotes the yield function, $\boldsymbol{\varepsilon}$ denotes the strain, $\boldsymbol{u}$ denotes the displacements, and $\boldsymbol{\lambda}$ denotes the plastic multipliers.

In a finite element context, the governing equations are discretized by introducing appropriate approximations for the variables involved [23], and the mathematical description containing Eqs. (1)-(4) can be expressed as:

$$\begin{aligned} &\text{maximize } \alpha \\ &\text{subject to } \boldsymbol{A\sigma}=\alpha\boldsymbol{p}+\boldsymbol{p}_{\mathbf{0}},\ F\left(\boldsymbol{\sigma}\right)\le 0 \end{aligned} \tag{5}$$

where $\boldsymbol{p}$ and $\boldsymbol{p}_0$ denote the proportional part to a scalar parameter α and constant part of the external load, respectively.

A feasible algorithm to assess the stability of a geo-structure is the strength reduction limit analysis [24]. In this case, Eq. (5) can be rewritten as:

$$\begin{aligned} &\text{maximize } 0 \\ &\text{subject to } \boldsymbol{A\sigma}=\boldsymbol{p}_{\mathbf{0}},\ F\left(\boldsymbol{\sigma}\right)\le 0 \end{aligned} \tag{6}$$

But as mentioned by Li and Wang [25], the numerical analysis using the conventional FELA with strength reduction method may identity misleading failure surfaces and incorrect volumes of sliding mass because of the mesh distortion. To alleviate this problem, the adaptive meshing is introduced into the FELA to deliver a narrower bound solution and a more accurate failure mechanism by using control variables [22, 26, 27]. The principles and procedures of this intelligent technique can be referred to Sloan [16]. In this study, the internal dissipation that calculates from the deviatoric stresses and strain rates is selected as the control variable for subsequent analysis.

2.2 Random field theory

Random field theory suggested by Vanmarcke [7] is an important tool modeling the spatial variability of soil properties and has the ability to generate more realistic spatial distributions of the random variables. Generally, a two dimensional stationary random filed is necessary for plane issues, which can be defined by three parameters, namely, mean value (μ), coefficient of variation (COV), and autocorrelation function. Among these parameters, the autocorrelation function is introduced to describe the correlation between spatial points since the value of a soil parameter at one point will present a certain correlation to the adjacent one, and the correlation depends on its relative distance. The single exponential autocorrelation function which has been widely used in geotechnical engineering is chosen here to characterize the spatial variability of a random variable and is given by:

$$\rho = \left(\Delta x, \Delta z\right) = \exp\left(-\frac{\left|x_i - x_j\right|}{h_x} - \frac{\left|z_i - z_j\right|}{h_z}\right) \tag{7}$$

where $\left(x_i, z_i\right)$ and $\left(x_j, z_j\right)$ denote the positions of a random variable, h_x and h_z denote the horizontal and vertical autocorrelation distances, respectively.

The discretization of the random field is indispensable when numerical techniques such as finite element or finite difference methods are employed [28]. At present, the methods for conducting this task can be mainly divided into three categories, including point methods, average-type methods, and series expansion methods. Thereinto, the KLE, one of the series expansion methods, which can give consideration to both computation efficiency and accuracy is adopted here [29, 30].

Considering a random field denoted by $H(x,\ z;\theta)$, where θ denotes the numerable variable corresponding to a possible realization of random field, the KLE gives a second-moment characterization of this random process in accordance with deterministic orthogonal functions and uncorrelated random variables:

$$H(x,\ z;\theta)=\mu+\sum_{i=1}^{\infty}\sigma\sqrt{\lambda_i}f_i(x,\ z)\xi_i(\theta) \tag{8}$$

where σ denotes the standard deviation, λ_i and $f_i(x,z)$ denote the eigenvalues and eigenfunctions of the autocorrelation function, respectively, and $\xi_i(\theta)$ denotes a set of uncorrelated random variables with zero mean and unit variance.

Generally, it is practical to truncate the series expansion at the *M*th term with a given accuracy:

$$H(x,\ z;\theta)=\mu+\sum_{i=1}^{M}\sigma\sqrt{\lambda_i}f_i(x,\ z)\xi_i(\theta) \tag{9}$$

where *M* is the number of truncation terms, which depends on the desired calculation accuracy and the autocorrelation function [31, 32].

As illustrated in Eq. (9), using KLE to simulate a random filed is based on the spectral decomposition of its autocovariance function which is bounded, symmetric, and positive definite. Hence, the essential step for realizing the discretization is to answer the λ_i and $f_i(x,z)$ from the Fredholm integral equation of the second term:

$$\int_{\Omega}\rho\left[(x_1,\ z_1),\ (x_2,\ z_2)\right]f_i(x_2,\ z_2)\,\mathrm{d}x_2\,\mathrm{d}z_2=\lambda_i f_i(x_1,\ z_1) \tag{10}$$

Ghanem and Spanos [33] proposed a feasible procedure to obtain the accurate eigenvalues and eigenfunctions. But it is worth noting that analytic solutions are difficult to appear when the autocorrelation function is complex, and the numerical methods such as the wavelet-Galerkin are required in this case [34].

In the above analysis, the random variables are considered to be normally distributed, and the Gaussian random field is thus generated to model the parameters with spatial variability. But the Gaussian model may not always applicable, especially when the random variables are strictly nonnegative. Combined with the existing site-specific data of geotechnical properties, a lognormal random field is applied here to avoid negative values, which has also been confirmed to perform well in geotechnical literature [28, 31, 35]. It is worth noting that the geotechnical properties are not limited to lognormal distribution, which is only used here for illustration. Herein, the standard deviation and mean of InH can be quantified as:

$$\sigma_{\mathrm{In}\,H} = \sqrt{\mathrm{In}\left(1+\sigma_H^2/\mu_H^2\right)} \tag{11}$$

$$\mu_{\mathrm{In}\,H} = \mathrm{In}\,\mu_H - 0.5\sigma_{\mathrm{In}\,H}^2 \tag{12}$$

In this way, Eq. (9) is reformulated as:

$$H(x,\ z;\theta) = \exp\left[\mu_{\mathrm{In}\,H} + \sum_{i=1}^{M} \sigma_{\mathrm{In}\,H}\sqrt{\lambda_i}\, f_i(x,\ z)\xi_i(\theta)\right] \tag{13}$$

2.3 Monte Carlo simulation

The MCS services as an unbiased approach for reliability analysis often producing accurate solution for general problems, which has long been popular in geotechnical engineering duo to its simple principle and reliable performance [36, 37]. In the framework of MCS, a series of random fields are generated in a manner satisfying the given probability distribution and correlation structure, and the response is evaluated for each generated set. This process is performed continuously until various statistical characteristics of the aimed issues are identified. As a result, the issues of interest can be well understood from a probabilistic point of view.

For an earth dam, the factor of safety $F_s(\boldsymbol{X})$ is defined as the ratio of resistant force $S(\boldsymbol{X})$ to the driving force $T(\boldsymbol{X})$ along a certain slip surface, where $\boldsymbol{X}$ denotes a set of random variables used to simulate the random filed, $\boldsymbol{X} = [X_1, X_2, ..., X_N]$. Then a performance function $g(\boldsymbol{X})$ is formulated to define the limit state:

$$g(\boldsymbol{X}) = S(\boldsymbol{X})/T(\boldsymbol{X}) - 1 = F_s(\boldsymbol{X}) - 1 \tag{14}$$

Further, the failure probability of the earth dam denoted as P_f can be calculated by the following integral:

$$P_f = P[g(\boldsymbol{X}) < 0] = \int_{g(\boldsymbol{X})<0} f_{\boldsymbol{X}}(\boldsymbol{X}) d\boldsymbol{X} \tag{15}$$

where $g(\boldsymbol{X}) < 0$ denotes the failure domain, and $f_{\boldsymbol{X}}(\boldsymbol{X})$ denotes the joint probability density function.

MCS is selected here to evaluate the P_f since it has the ability to quantify the integral of Eq. (15) via a large number of simulations, and P_f can be therefore given as:

$$P_f = \frac{1}{N_{\mathrm{MCS}}} \sum_{i=1}^{N_{\mathrm{MCS}}} I_{\mathrm{MCS}}(\boldsymbol{X}) = \frac{N_{fail}}{N_{\mathrm{MCS}}} \tag{16}$$

where N_{MCS} denotes the number of MCS, $I_{\mathrm{MCS}}(\boldsymbol{X})$ denotes the event of failure of the earth dam, when the dam fails, $I_{\mathrm{MCS}}(\boldsymbol{X}) = 1$ and $I_{\mathrm{MCS}}(\boldsymbol{X}) = 0$ otherwise, and N_{fail} denotes the total failure events in N_{MCS}.

2.4 Risk assessment

Risk assessment considers not only the probability of failure but also the consequence, which evaluates the safety of structures in a quantitative manner [4]. Mathematically, the risk assessment can be defined as the product of the failure probability and consequence [4, 5]:

$$R = P_f C \tag{17}$$

where R denotes the risk, and C denotes the failure consequence termed as the sliding mass of the earth dam here.

But the above equation is specific to the earth dams with only one failure mode. When the spatial variability of material parameters is included, there are numerous potential failure modes for an earth dam. The consequence for the deep failure is obviously greater than that of shallow, so the risk assessment needs to be extended considering the consequence associated with each failure mode individually. In this end, a modified definition with regards to the Eq. (17) is rewrote in a MCS framework [4, 5, 38]:

$$R = \sum_{i=1}^{N_{fail}} P_{fi} C_i = \sum_{i=1}^{N_{fail}} \frac{1}{N_{\mathrm{MCS}}} C_i = \frac{1}{N_{\mathrm{MCS}}} \sum_{i=1}^{N_{fail}} C_i = \frac{N_{fail}}{N_{\mathrm{MCS}}} \frac{\sum_{i=1}^{N_{fail}} C_i}{N_{fail}} = P_f \overline{C} \tag{18}$$

where P_{fi} and C_i denote the probability and corresponding consequence of the ith failure respectively, and $\overline{C}$ denotes the average consequence among the failures.

Comparing the Eqs. (17) and (18), it can be found that the expressions are consistent except for that the modified definition uses the average consequence of all failure modes instead of individual consequence. In the context of risk assessment, the P_f can be answered by MCS mentioned above, and consequence of each failure mode can be given by *K*-means clustering method [4, 39].

3. Implementation procedure

In order to facilitate the understanding of the implementation procedure of RAFELA, a flowchart that illustrates the specific steps is showed in Fig. 2. In general, seven steps are needed in this procedure, and details of each step are summarized as follows:

(1) Determine deterministic parameters and spatially varying variables, including but not limited to model configuration, site-specific information, and statistical characteristics that can be characterized by a set of prior knowledge, such as means, distributions, coefficients of variation (COVs), autocorrelation functions, and autocorrelation distances.

(2) Discretize the lognormal random fields by means of KLE to characterize the spatial variability, in which the truncation term M in KLE is set to a suitable value to achieve a relatively accurate random field representation [40]. Then, a realization of the underlying Gaussian random fields is modeled.

(3) Run the RAFELA software with the above given geometrical and geotechnical input parameters. In this study, Optum G2 is employed to perform the numerical analysis, and bound solution is obtained in each realization with the discrete random fields.

(4) Generate the independent standard normal random sample vector $\xi_i(\theta)$ for N_{MCS} times, and achieve N_{MCS} realizations of the underlying Gaussian random fields.

(5) Repeat the numerical calculation N_{MCS} times using the random fields generated above, and N_{MCS} output files containing factors of safety, failure modes, and consequences for each realization are obtained.

(6) Extract the factors of safety and consequences from the N_{MCS} output files, and the failure events that the values of F_s are below 1.0 are denoted as N_{fail}. Hence, the P_f is given by $P_f = N_{fail} / N_{\mathrm{MCS}}$, and the $\overline{C}$ is given by $\overline{C} = \sum_{i=1}^{N_{fail}} C_i \Big/ N_{fail}$.

(7) Assess the risk of the earth dam failure by the product of the probability of failure and the

average consequence among the failures, so the R can be expressed as $R = P_f \overline{C}$.

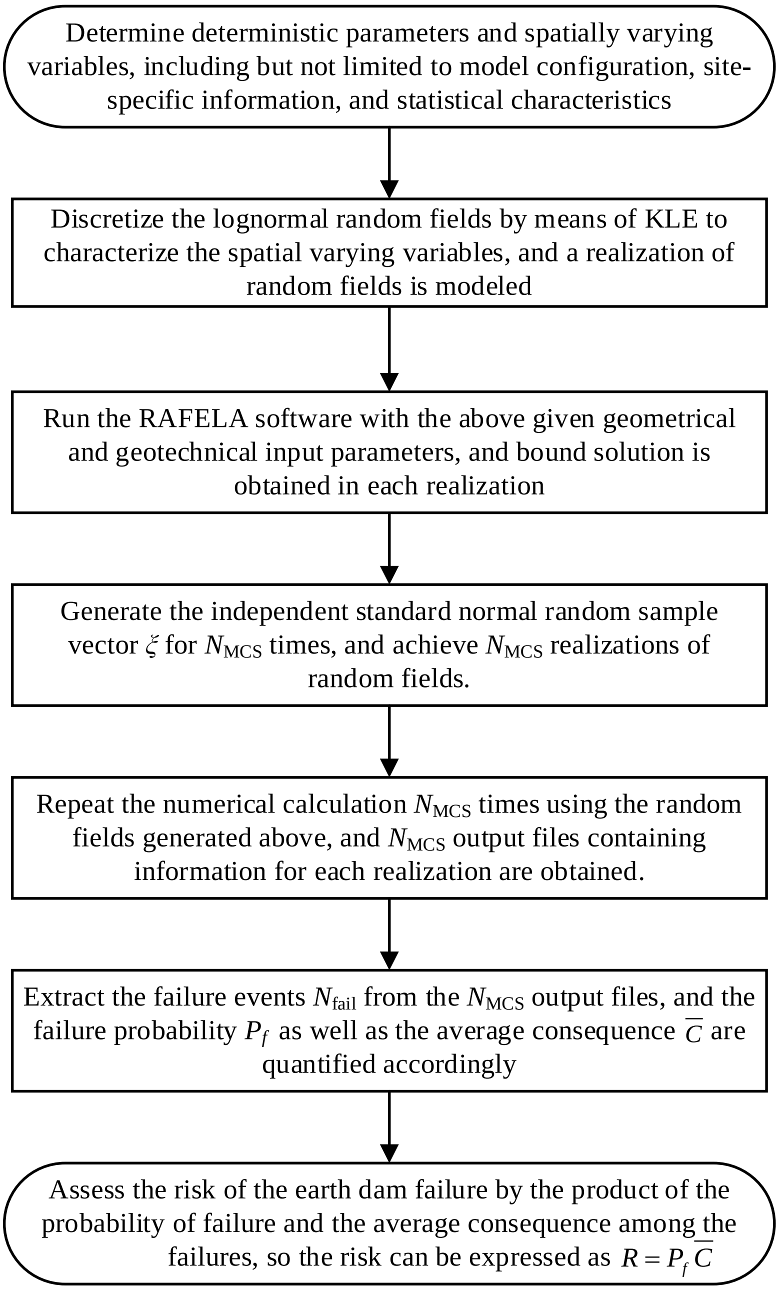

Fig. 2 Flowchart of the implementation procedure for the RAFELA

4. Case study

4.1 Deterministic analysis

The earth dam presented here is shown in Fig. 3, which consists of an embankment on a soil foundation. The embankment has a height of 10 m with upstream and downstream slopes of 2 h:1 v, and the foundation is also 10 m high. The reservoir water level is 9 m above the foundation. A horizontal under-drain is specified at the toe of the downstream slope to maintain the water level at the tail water elevation for a distance of 5 m near the embankment toe.

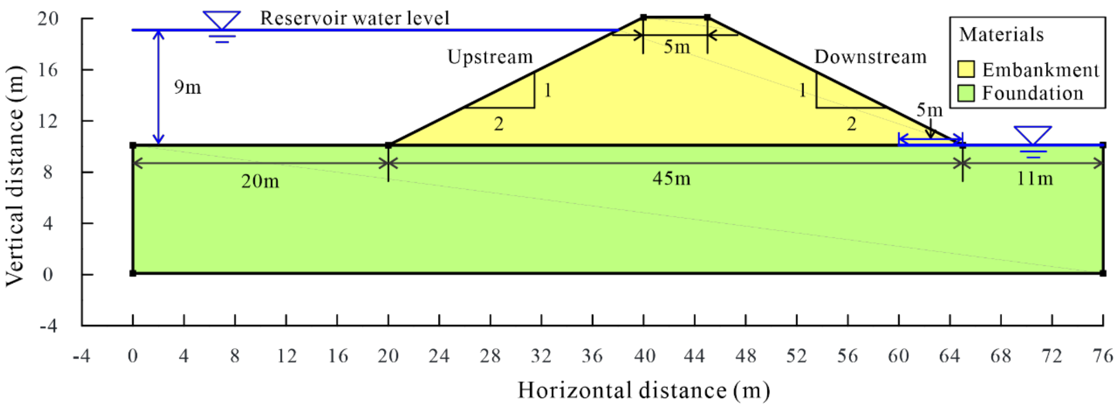

Fig. 3 The geometry of the earth dam

Prior to performing the probabilistic analysis that takes the spatial variability of stochastic parameters into account, a deterministic calculation with mean input parameters is conducted to study the seepage behavior and stability of the dam. The soils properties in embankment and foundation are presented in Table 1. Adaptive meshing is employed in all analyses, where the default option of shear dissipation is selected as the adaptivity control to refine the mesh, and three adaptive iterations are defined for acquiring an accurate solution. An initial mesh of 1,000 elements is specified here and then a final mesh of 10,000 elements is generated according to the results of iterations.

Table 1 Deterministic soil parameters for the case study

Soil properties	Embankment	Foundation
Unit weight γ (kN/m^3)	19	20
Cohesion c (kPa)	10	15
Internal friction angle φ (°)	20	23
Saturated hydraulic conductivity K_s (m/d)	0.1	0.1
Saturated water content θ_s (%)	50	50
Residual water content θ_r (%)	5	5
Poisson's ratio υ	0.334	0.334
Elasticity modulus E (MPa)	5	5

Figure 4 shows the saturation distribution of the earth dam subjected to the reservoir water level. In particular, the van Genutchen model is used to describe the soil-water characteristic curve involved in seepage analysis [41], and the model parameters α_{vG} and n_{vG} are 0.62 and 1.11, respectively. The saturation distribution obtained here is highly consistent with the SEEP/W that has the same model configuration and hydraulic parameters, in which the minimum degree of the saturation on the downstream is 0.712 in AFELA and 0.713 in SEEP/W [42].

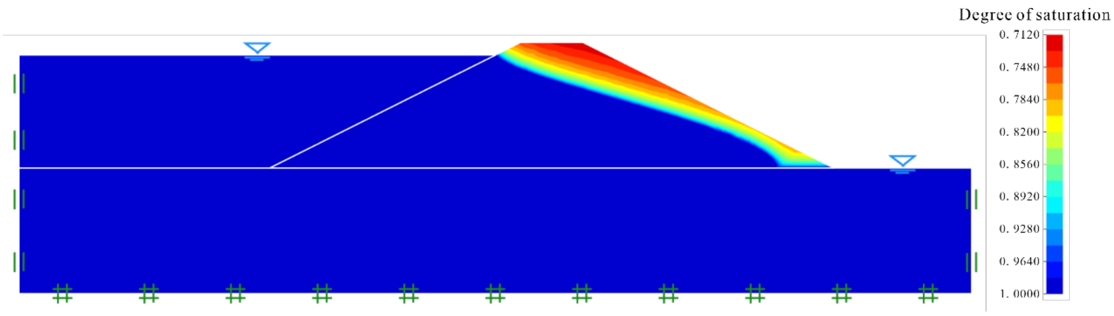

Fig. 4 The degree of saturation of the earth dam subjected to the reservoir water level

Further, the stability of the earth dam is calculated based on the results from the seepage field. As the LB is at the safe side, it is chosen as the basis for subsequent analysis to reduce the computational consumption. As shown in Fig. 5, the factor of safety is 1.217 in the AFELA. The failure surface of the earth dam and the adapted meshes for approximately 10,000 elements in the numerical analysis are also illustrated in Fig. 5. It can be found that the mesh density near the phreatic line and the failure surface is relatively high, which is due to the automatic optimization iterations and helps to get a more accurate solution.

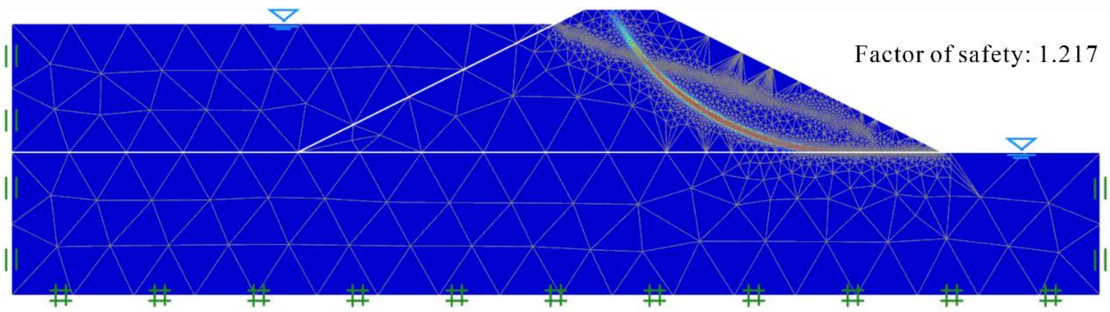

Fig. 5 The stability of the earth dam in the AFELA

4.2 Stochastic analysis

In this section, the stochastic response for the earth dam is illustrated considering the spatial variability of strength parameters. The specific statistical properties of the soil parameters in the embankment and foundation are shown in Table 2. Particularly, c and φ are thought to be statistically independent, and the strength parameters are assumed have the same autocorrelation distance in horizontal and vertical directions.

Table 2 Statistical properties of the strength parameters

Strength parameters	Mean value		COV	h_x (m)	h_z (m)	Distribution
	Embankment	Foundation				
c (kPa)	10	15	0.3	20	2	Lognormal
φ (°)	20	23	0.15	20	2	Lognormal

Once the statistical properties are determined, the random fields of the strength parameters can be generated by the KLE. Meanwhile, in order to model a relatively accurate random field, the truncation term M in the KLE is set to 1,000. Figure 6 illustrates a realization of the random fields implemented in the stochastic analysis.

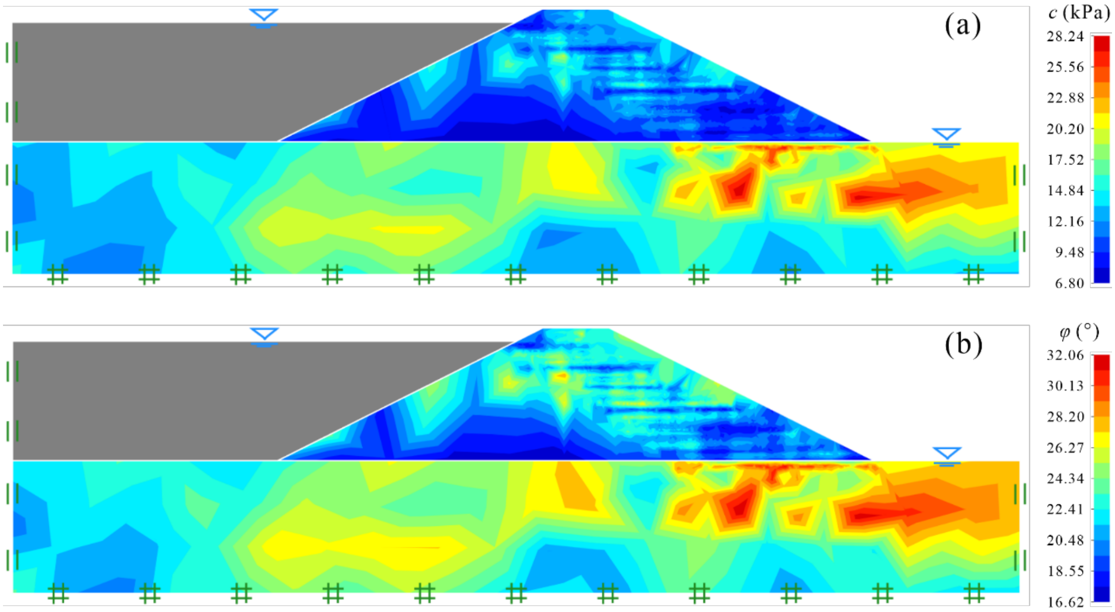

Fig. 6 A realization of the random fields. (a) c. (b) φ

Further, the approach for quantifying the statistical response is conducted through MCS. A series of random fields are modeled in a manner consistent with the correlation structure of the variables, and each set of random fields produces a deterministic solution. This process will continue until the P_f is basically stable and unaffected by a single extreme event. Theoretically, the result can be more reliable as the number of implementations increases. Herein, after balancing the efficiency of the calculation and the accuracy of the results, two thousand simulations are performed for the cases where P_f is larger than 10%, and more simulations are added for other cases to ensure that the maximum error in P_f is less than 0.01 at a confidence level of 90%.

Consequently, the P_f is 15.1%, which means that a total of 302 failure events occur in 2,000 simulations. In more detail, the probability distributions of the factor of safety, including the histogram of the relative frequency and cumulative probability, are presented in Fig. 7. In contrary to the deterministic analysis that a single factor of safety is obtained, the stochastic analysis can provide more information, especially the statistical characteristics of the stability, which helps to deepen the understanding of the overall permanence of the earth dam from the perspective of probability.

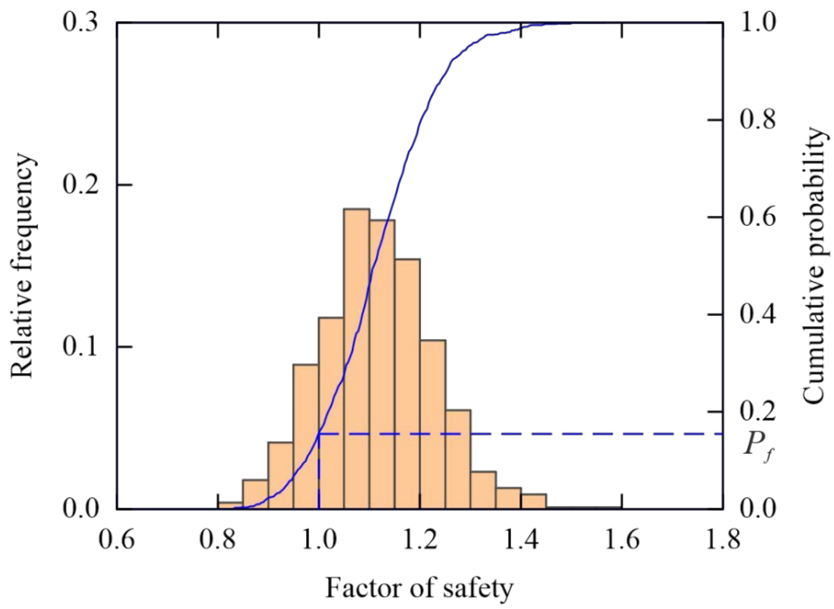

Fig. 7 Probability distributions of factor of safety

In addition to the factors of safety, a large number of failure modes are also identified simultaneously. Figure 8 shows three typical failure modes, namely shallow failure, intermediate failure, and deep failure. Intrinsically, the diversity of the dam failure here comes from the spatial variability of the soils, which partly explains the uncertainty of the failure occurrence in actual observation.

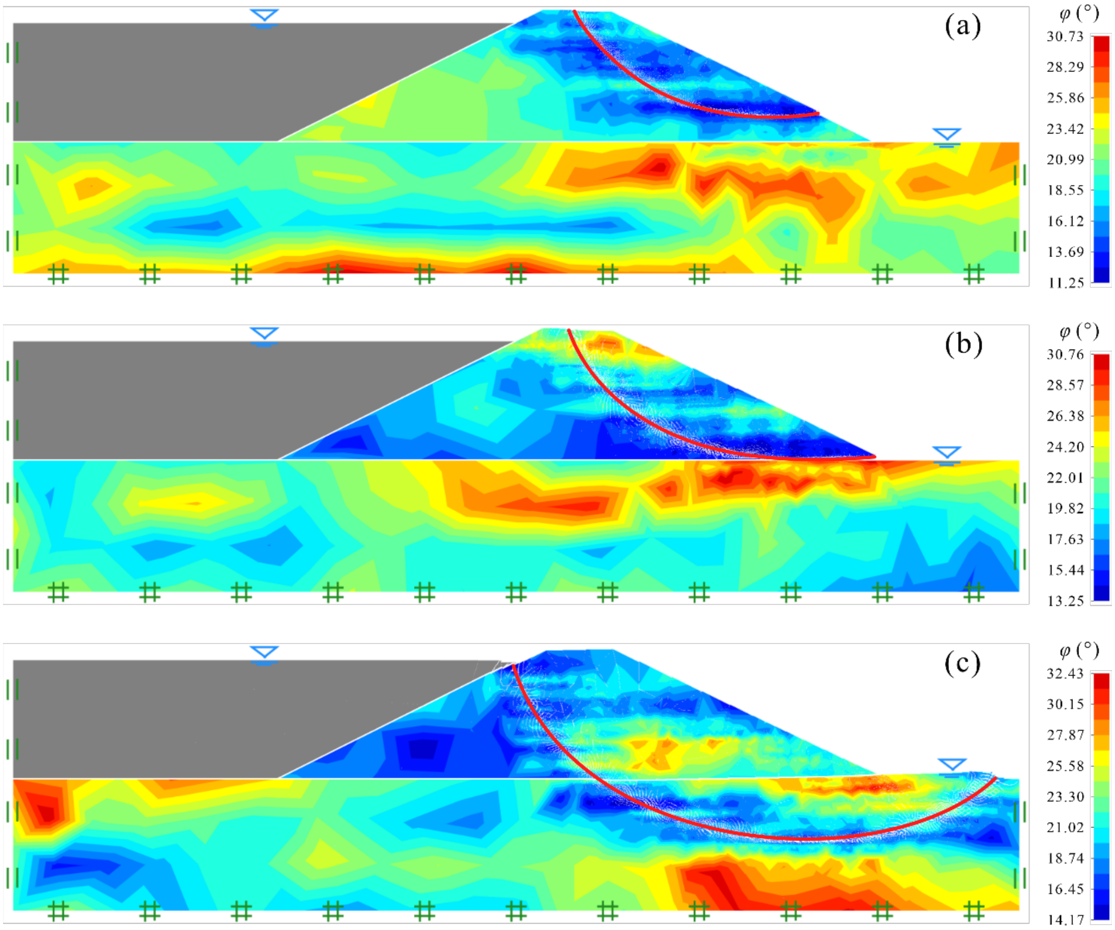

Fig. 8 Typical failure modes of the spatially variable earth dam. (a) shallow failure. (b) intermediate failure. (c) deep failure

The consequences associated with above three failure modes are quite different. According to the Eq. (18), it is necessary to evaluate the consequence for each failure event individually, and the average consequence among these failures can therefore be obtained. The average consequence is calculated to be 125.5 m^2 in a total of 302 failures. Finally, the risk of the earth dam failure can be quantified by the product of the failure probability and average consequence, and the result is 18.95 m^2.

5. Discussion

When modeling the random field, several parameters of the correlation structure, such as the COV, h_x, and h_z, are indispensable. Regarding the values of these parameters are mostly empirical and trial owing to lack of sufficient data, which are therefore necessary to have further discussion.

5.1 Effects of the COV

For the stochastic analysis above, the COVs of c and φ are set to 0.3 and 0.15, respectively. In fact, it is strenuous to determine its exact value because a great deal of effort must be put into testing the site information. Therefore, eight groups of different parameters are taken to investigate the effects of the COVs of c and φ on the stochastic response and risk assessment, including 0.15, 0.3, 0.45, and 0.6 for c, and 0.1, 0.15, 0.2 and 0.25 for φ.

As shown in Figs. 9 and 10, the probability distributions of factor of safety for different COVs of c and φ are presented. The P_f rises from 3.7% to 39.7% when the COV of c increases from 0.15 to 0.6, and rises from 6.8% to 34% when the COV of φ increases from 0.1 to 0.25. It is worth noting that the results here and later are given by treating the stochastic parameters of the embankment and foundation as simultaneous variations.

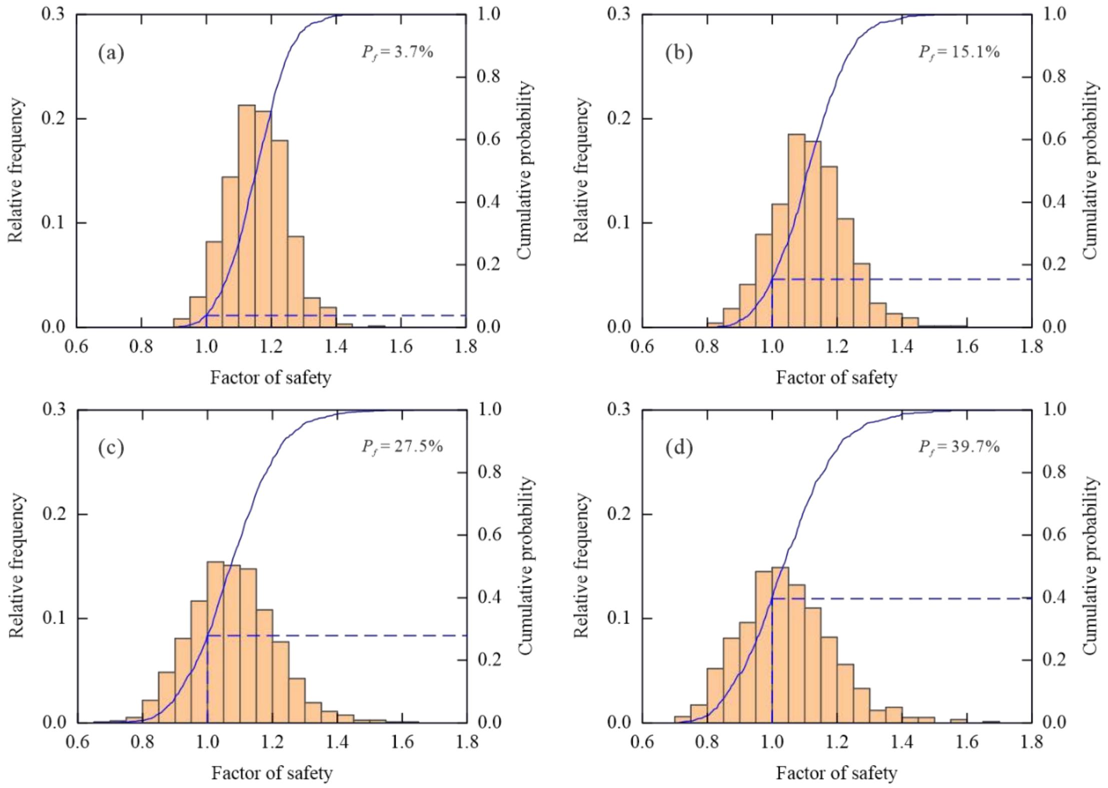

Fig. 9 Probability distributions of factor of safety for different COV of *c*. (a) The COV of *c* is 0.15. (b) The COV of *c* is 0.3. (c) The COV of *c* is 0.45. (d) The COV of *c* is 0.6

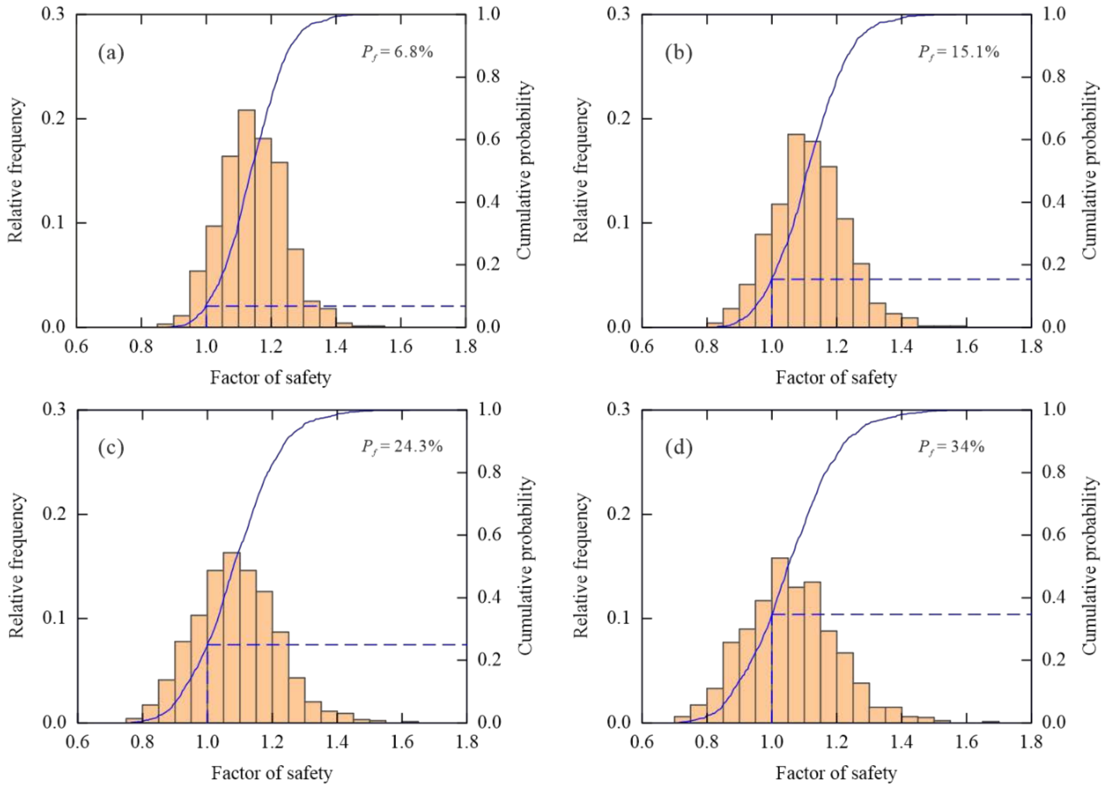

Fig. 10 Probability distributions of factor of safety for different COV of φ. (a) The COV of φ is 0.1. (b) The COV of φ is 0.15. (c) The COV of φ is 0.2. (d) The COV of φ is 0.25

Subsequently, the risk assessment of the earth dam failure is summarized in Table 3. Similar to the P_f, the R rises with the increase of the COVs of c and φ. Particularly, the R reaches 55.2 m^2 when the COV of c increases to 0.6, and reaches 47.37 m^2 when the COV of φ increases to 0.25. Both the P_f and R indicate that the COVs of c and φ have a significant impact on the dam failure, so more attention should be paid to measuring these two parameters.

Table 3 Risk assessment of the earth dam for different COVs of c and φ

COV	c	φ

	0.15	0.3	0.45	0.6	0.1	0.15	0.2	0.25
R (m^2)	4.46	19.41	35.85	55.2	7.93	19.41	32.82	47.37

5.2 Effects of the h_x and h_z

The autocorrelation distance is used to describe the spatial extent that the soil properties are significantly correlated. A large autocorrelation distance suggests a smoothly varying field over a large spatial extent whereas the opposite implies a more ragged field thus less uniformity in the soil properties. In general, the autocorrelation distance is decomposed in two directions, horizontal and vertical. Although the exact values are hard to come by, previous studies have shown that the h_x is much greater than the h_z [43, 44]. Likewise, in order to investigate the effects of the h_x and h_z on the stochastic response and risk assessment, eight groups of different parameters are taken, including 10 m, 15 m, 20 m, and 40 m for horizontal direction, and 1 m, 1.5 m, 2 m, and 4 m for vertical direction, respectively.

It can be observed from Figs. 11 and 12 that the P_f rises as the autocorrelation distance increases, which would be expected. A larger autocorrelation distance suggests a stronger correlation of the random variables and generates a smaller fluctuation of the simulated values when modeling the random field. The average simulated values vary a lot from one realization to another in this case, leading to a more spread-out distribution of the factor of safety. As a result, the P_f rises from 10.6% to 16.9% when the h_x increases from 10 m to 40 m, and rises from 11.8% to 16.5% when the h_z increases from 1 m to 4 m.

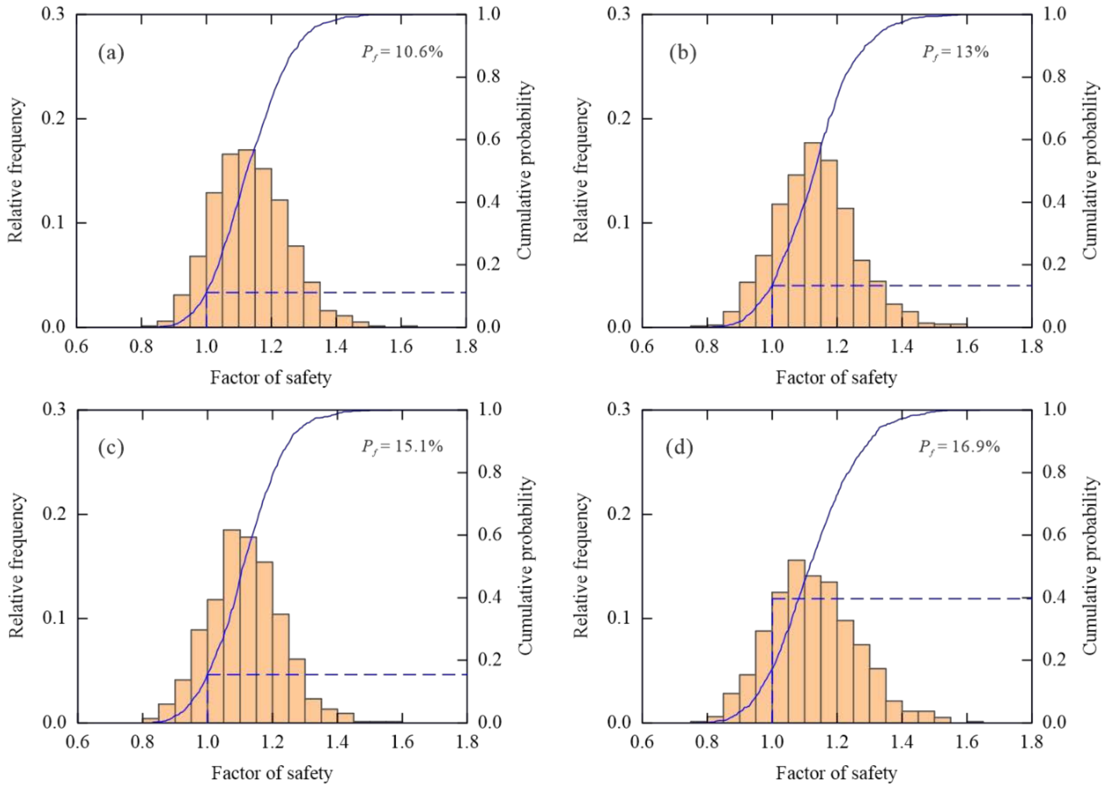

Fig. 11 Probability distribution of factor of safety for different h_x. (a) The h_x is 10 m. (b) The h_x is 15 m. (c) The h_x is 20 m. (d) The h_x is 40 m

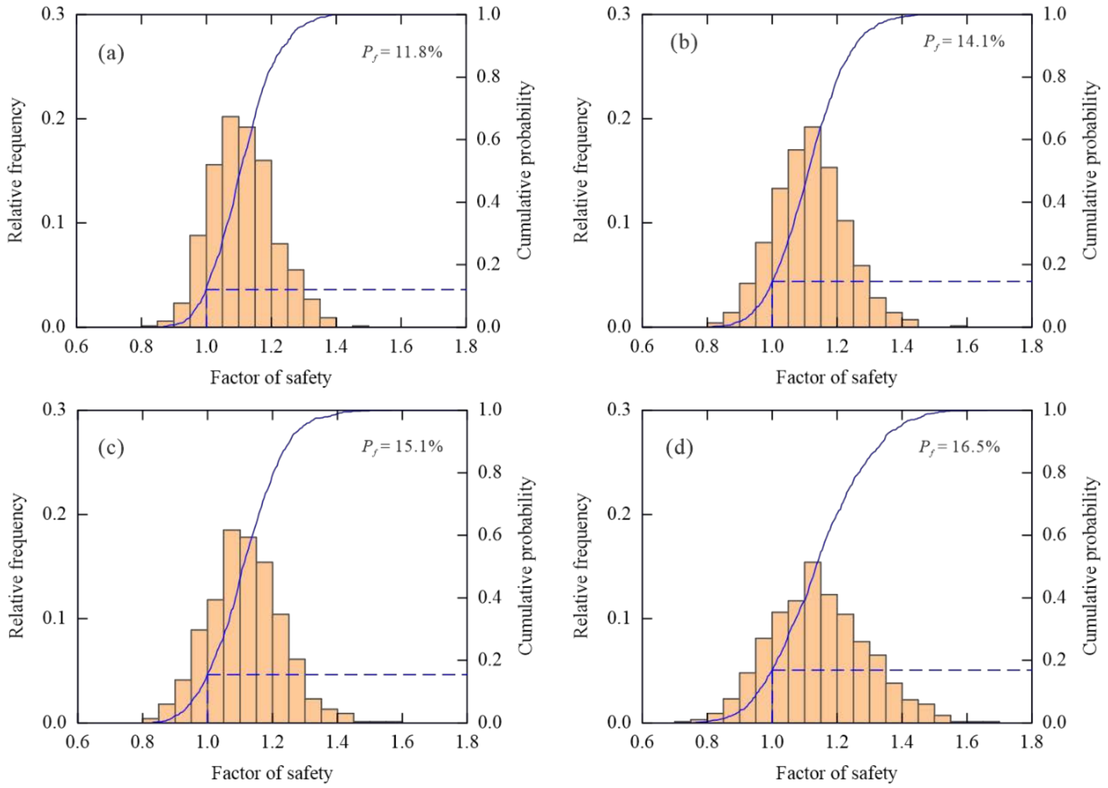

Fig. 12 Probability distribution of factor of safety for different h_z. (a) The h_z is 1 m. (b) The h_z is 1.5 m. (c) The h_z is 2 m. (d) The h_z is 4 m

Further, the risk assessment of the earth dam failure for different h_x and h_z is summarized in Table 4. It can be seen that increasing the h_x and h_z increases both the P_f and R, respectively. Meanwhile, by comparing the Tables 3 and 4, it can be inferred that the stochastic response and risk assessment are more sensitive to the COVs of c and φ than that of the h_x and h_z.

Table 4 Risk assessment of the earth dam for different h_x and h_z

Autocorrelation	h_x				h_z			
distance (m)	10	15	20	40	1	1.5	2	4
R (m^2)	13.24	17.01	19.41	22.8	15.06	18.14	19.41	20.94

6. Conclusions

This study presents a risk assessment for an earth dam in spatially variable soils using RAFELA. The spatial variability of soils, mainly the strength parameters, is described by the random field theory. Then the stochastic analysis is implemented through unbiased MCS in the efficient AFELA framework, and the failure probability and the average consequence among the failures are obtained. Subsequently, the risk of the earth dam failure is assessed by the product of the failure probability and the average consequence. In contrary to the deterministic analysis that only a failure mode and a factor of safety are obtained, the stochastic analysis considering the spatial variability can deliver a wide range of failure modes and assess the risk of the earth dam failure comprehensively, which can be served as a theoretical basis for further decision-making and mitigation.

The effects of the correlation structure of strength parameters on the stochastic response and risk assessment are investigated by performing a series of parametric analyses. Both the P_f and R of the earth dam rise with the increase of parameters in correlation structure. The stochastic response and risk assessment are more sensitive to the COVs of c and φ than that of the h_x and h_z. As a guide, in the actual investigation of site spatial properties, measures should be taken to pay more attention to the influential parameters, which can help deepen the understanding of the overall performance of the structure.

Acknowledgement

This research is supported by the National Natural Science Foundation of China (No. 41977244 and No. 42007267). The first author is supported by China Scholarship Council (CSC) as a visiting scholar at the Leibniz University Hannover, under grant No. 202006410089. All supports are gratefully acknowledged.

Declaration of Competing Interest

The authors declare that they have no known competing financial interests or personal relationships that could have appeared to influence the work reported in this paper.

References

1. Zhang L, Peng M, Chang D, Xu Y (2016) Dam Failure Mechanisms and Risk Assessment. John Wiley & Sons, Singapore
2. Guo X, Dias D, Carvajal C, Peyras L, Breul P (2021) Modelling and comparison of different types of random fields: case of a real earth dam. Eng Comput. https://doi.org/10.1007/s00366-021-01495-4
3. Liu X, Wang Y, Li DQ (2019) Investigation of slope failure mode evolution during large deformation in spatially variable soils by random limit equilibrium and material point methods. Comput Geotech 111:301–312. https://doi.org/10.1016/j.compgeo.2019.03.022
4. Huang J, Lyamin AV, Griffiths DV, Krabbenhoft K, Sloan SW (2013) Quantitative risk assessment of landslide by limit analysis and random fields. Comput Geotech 53:60–67. https://doi.org/10.1016/j.compgeo.2013.04.009

5. Jiang SH, Huang JS, Griffiths DV, Deng ZP (2022) Advances in reliability and risk analyses of slopes in spatially variable soils: A state-of-the-art review. Comput Geotech 141:104498. https://doi.org/10.1016/j.compgeo.2021.104498
6. Cheng H, Chen J, Chen R, Chen G, Zhong Y (2018) Risk assessment of slope failure considering the variability in soil properties. Comput Geotech 103:61–72. https://doi.org/10.1016/j.compgeo.2018.07.006
7. Vanmarcke EH (2010) Random Fields: Analysis and Synthesis. World Scientific Publishing Co Pte Ltd, Singapore
8. Griffiths DV, Fenton GA (2004) Probabilistic slope stability analysis by finite elements. J Geotech Geoenviron Eng 130(5):507–518. https://doi.org/10.1061/(ASCE)1090-0241(2004)130:5(507)
9. Griffiths DV, Huang J, Fenton GA (2009) Influence of spatial variability on slope reliability using 2-D random fields. J Geotech Geoenviron Eng 135(10):1367–1378. https://doi.org/10.1061/(ASCE)GT.1943-5606.0000099
10. Hicks MA, Nuttall JD, Chen J (2014) Influence of heterogeneity on 3D slope reliability and failure consequence. Comput Geotech 61:198–208. https://doi.org/10.1016/j.compgeo.2014.05.004
11. Gholampour A, Johari A (2019) Reliability-based analysis of braced excavation in unsaturated soils considering conditional spatial variability. Comput Geotech 115:103163. https://doi.org/10.1016/j.compgeo.2019.103163
12. Jiang SH, Liu X, Huang J (2020) Non-intrusive reliability analysis of unsaturated embankment slopes accounting for spatial variabilities of soil hydraulic and shear strength parameters. Eng

Comput. https://doi.org/10.1007/s00366-020-01108-6

13. Xue Y, Miao F, Wu Y, Li L, Meng J (2021) Application of uncertain models of sliding zone on stability analysis for reservoir landslide considering the uncertainty of shear strength parameters. Eng Comput. https://doi.org/10.1007/s00366-021-01446-z

14. Tabarroki M, Ching J (2019) Discretization error in the random finite element method for spatially variable undrained shear strength. Comput Geotech 105:183–194. https://doi.org/10.1016/j.compgeo.2018.10.001

15. Chwała M (2021) Upper-bound approach based on failure mechanisms in slope stability analysis of spatially variable c-φ soils. Comput Geotech 135:104170. https://doi.org/10.1016/j.compgeo.2021.104170

16. Sloan SW (2013) Geotechnical stability analysis. Geotechnique 63(7):531–572. https://doi.org/10.1680/geot.12.RL.001

17. Ali A, Lyamin AV, Huang J, Sloan SW, Cassidy MJ (2017) Undrained stability of a single circular tunnel in spatially variable soil subjected to surcharge loading. Comput Geotech 84:16–27. https://doi.org/10.1016/j.compgeo.2016.11.013

18. Zhou H, Liu H, Yin F, Chu J (2018) Upper and lower bound solutions for pressure-controlled cylindrical and spherical cavity expansion in semi-infinite soil. Comput Geotech 103:93–102. https://doi.org/10.1016/j.compgeo.2018.07.011

19. Tang C, Phoon K (2019) Prediction of bearing capacity of ring foundation on dense sand with regard to stress level effect. Int J Geomech 18(11):04018154. https://doi.org/10.1061/(ASCE)GM.1943-5622.0001312

20. Wu G, Zhao H, Zhao M, Zhu Z (2021) Stochastic analysis of dual tunnels in spatially random

soil. Comput Geotech 129:103861. https://doi.org/10.1016/j.compgeo.2020.103861

21. Lyamin AV, Sloan SW (2003) Mesh generation for lower bound limit analysis. Adv Eng Softw 34(6):321–338. https://doi.org/10.1016/S0965-9978(03)00032-2
22. Lyamin AV, Sloan SW, Krabbenhøft K, Hjiaj M (2005) Lower bound limit analysis with adaptive remeshing. Int J Numer Meth Eng 63(14):1961–1974. https://doi.org/10.1002/nme.1352
23. Krabbenhoft K, Lyamin AV, Hjiaj M, Sloan SW (2005) A new discontinuous upper bound limit analysis formulation. Int J Numer Methods Eng 63:1069–1088. https://doi.org/10.1002/nme.1314
24. Krabbenhoft K, Lyamin AV (2015) Strength reduction finite-element limit analysis. Geotech Lett 5(4):250–253. https://doi.org/10.1680/jgele.15.00110
25. Li L, Wang Y (2020) Identification of failure slip surfaces for landslide risk assessment using smoothed particle hydrodynamics. Georisk 14(2):91-111. https://doi.org/10.1080/17499518.2019.1602877
26. Borges L, Zouain N, Costa C, Feijóo R (2001) An adaptive approach to limit analysis. Int J Solids Struct 38:1707–1720. https://doi.org/10.1016/S0020-7683(00)00131-1
27. Ciria H, Peraire J, Bonet J (2008) Mesh adaptive computation of upper and lower bounds in limit analysis. Int J Numer Methods Eng 75:899–944. https://doi.org/10.1002/nme.2275
28. Cho SE (2014) Probabilistic stability analysis of rainfall-induced landslides considering spatial variability of permeability. Eng Geol 171:11–20. https://doi.org/10.1016/j.enggeo.2013.12.015
29. Zhang D, Lu Z (2004) An efficient, high-order perturbation approach for flow in random porous media via Karhunen–Loève and polynomial expansions. J Comput Phys 194(2):773–

794. https://doi.org/10.1016/j.jcp.2003.09.015

30. Yang HQ, Zhang L, Xue J, Zhang J, Li X (2019) Unsaturated soil slope characterization with Karhunen-Loève and polynomial chaos via Bayesian approach. Eng Comput 35(1):337–350. https://doi.org/10.1007/s00366-018-0610-x

31. Jiang SH, Li DQ, Zhang LM, Zhou CB (2014) Slope reliability analysis considering spatially variable shear strength parameters using a non-intrusive stochastic finite element method. Eng Geol 168:120–128. https://doi.org/10.1016/j.enggeo.2013.11.006

32. Jiang SH, Li DQ, Cao ZJ, Zhou CB, Phoon KK (2015) Efficient system reliability analysis of slope stability in spatially variable soils using Monte Carlo simulation. J Geotech Geoenviron Eng 141(2):04014096. https://doi.org/10.1061/(ASCE)GT.1943-5606.0001227

33. Ghanem R, Spanos PD (1991) Stochastic Finite Element: A Spectral Approach. Springer-Verlag, New York

34. Phoon KK, Huang SP, Quek ST (2002) Implementation of Karhunen-Loeve expansion for simulation using a wavelet-Galerkin scheme. Probab Eng Mech 17(3):293–303. https://doi.org/10.1016/S0266-8920(02)00013-9

35. Bozorgpour MH, Binesh SM, Rahmani R (2021) Probabilistic stability analysis of geo-structures in anisotropic clayey soils with spatial variability. Comput Geotech 133:104044. https://doi.org/10.1016/j.compgeo.2021.104044

36. Li DQ, Jiang SH, Cao ZJ, Zhou W, Zhou CB, Zhang LM (2015) A multiple response surface method for slope reliability analysis considering spatial variability of soil properties. Eng Geol 187:60–72. https://doi.org/10.1016/j.enggeo.2014.12.003

37. Liao K, Wu YP, Miao FS, Li LW, Xue Y (2021) Time-varying reliability analysis of Majiagou

landslide based on weakening of hydro-fluctuation belt under wetting-drying cycles. Landslides 18(1):267-280. https://doi.org/10.1007/s10346-020-01496-2

38. Jiang SH, Huang J, Yao C, Yang J (2017) Quantitative risk assessment of slope failure in 2-D spatially variable soils by limit equilibrium method. Appl Math Model 47:710–725. https://doi.org/10.1016/j.apm.2017.03.048

39. Bishop CM (2006) Pattern recognition and machine learning. Springer, Berlin

40. Wang ZZ, Xiao C, Goh SH, Deng MX (2021) Metamodel-Based Reliability Analysis in Spatially Variable Soils Using Convolutional Neural Networks. J Geotech Geoenviron Eng 147(3):04021003. https://doi.org/10.1061/(ASCE)GT.1943-5606.0002486

41. van Genuchten, MT (1980) A closed form equation for predicting the hydraulic conductivity of unsaturated soils. Soil Sci Soc Am J 44(5):892–898. http://dx.doi.org/10.2136/sssaj1980.03615995004400050002x

42. Krahn J (2004) Seepage modeling with SEEP/W: an engineering methodology. GEO-SLOPE International Ltd, Calgary, Alberta, Canada

43. El-Ramly H, Morgenstern NR, Cruden DM (2003) Probabilistic stability analysis of a tailings dyke on presheared clay-shale. Can Geotech J 40:192–208. https://doi.org/10.1139/t02-095

44. Phoon KK, Kulhawy FH (1999) Characterization of geotechnical variability. Can Geotech J 36(4):612–624. https://doi.org/10.1139/t99-038